Electronic Supplementary Material (ESI) for Journal of Materials Chemistry A.

Electronic Supplementary Information

Kinetically Controlled Redox Behaviors of $K_{0.3}MnO_2$ Electrodes for High Performance Sodium-Ion Batteries

*Jiasheng Qian, Ying San Chui, Guijun Li, Mei Lin, Chi Man Luk, Chun Hin Mak, Biao Zhang, Feng Yan and Shu Ping Lau**

List of Contents

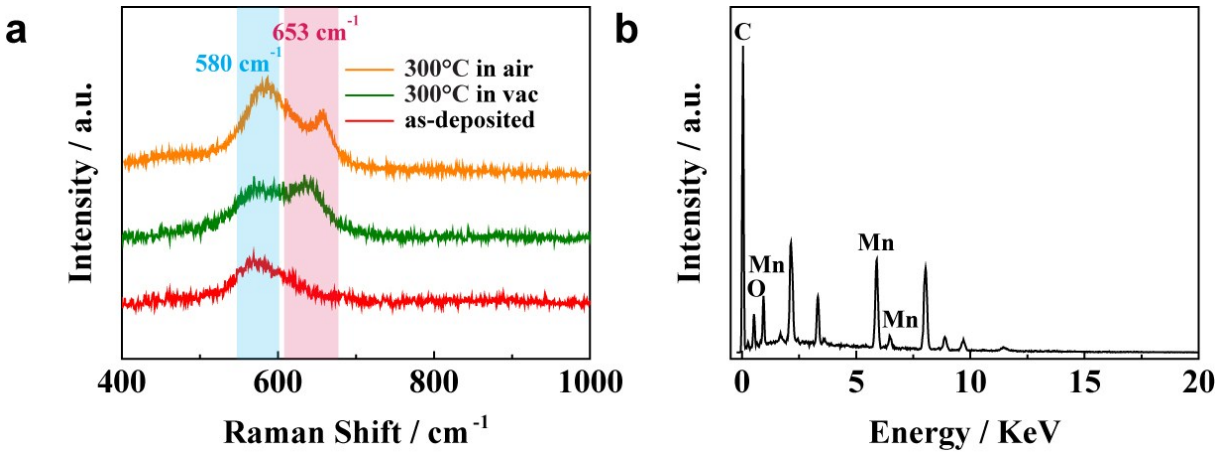

Fig. S1 Characterizations of the $K_{0.3}MnO_2$ nanosheets. a) Raman spectra at various conditions. b) EDX pattern. To increase the sample conductivity, gold was coated on the surface. The EDX pattern demonstrates the existence of massive manganese, oxygen and potassium element.

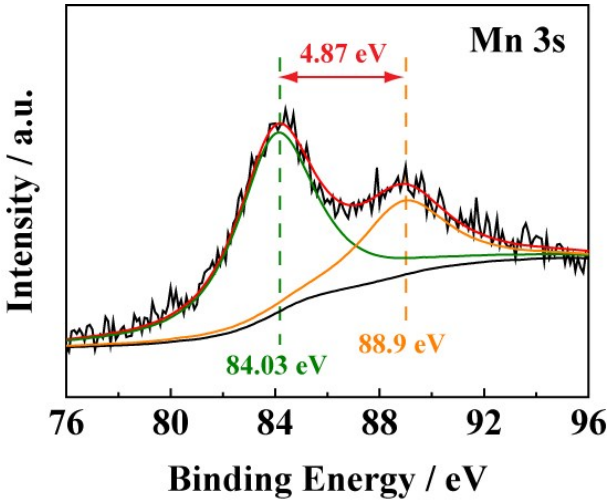

Fig. S2 XPS spectrum of the $K_{0.3}MnO_2$ nanosheets corresponding to the Mn 3s state.

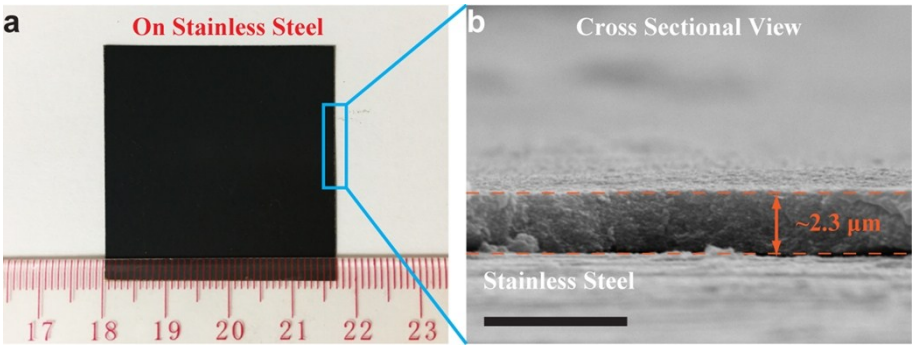

Fig. S3 Optical and cross-sectional SEM images of the R-MnNS electrodes on stainless steel (SS) sheet. a) Optical photograph of the surface view of the R-MnNS electrode on SS sheet. b) SEM image of the cross-sectional view of the R-MnNS electrode. Scale bar is 5 µm.

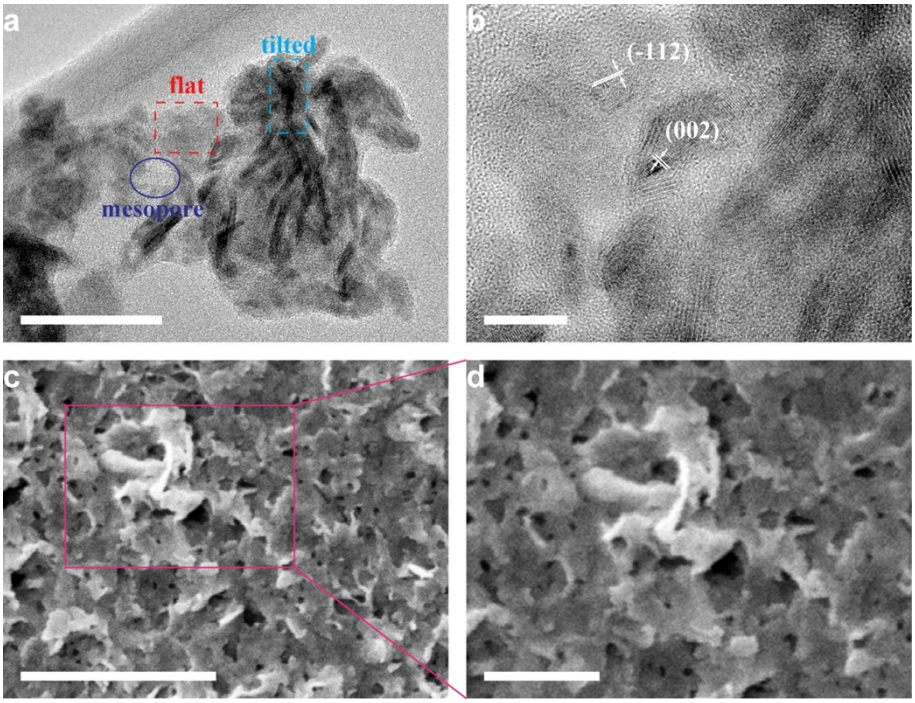

Fig. S4 Surface morphology of the R-MnNS electrode. a, b) High-resolution TEM images. Scale bars are 50 nm for panel a and 10 nm for panel b. As shown in Figure a, both flat (in red dash lines) and tilted (in azure dash lines) $K_{0.3}MnO_2$ nanosheets could be observed. Lattice fringes could be observed from Figure b, which could be assigned to the (-112) and (002) reflections of the K-birnessite MnO_2. c, d) High-resolution SEM images. Scale bars are 500 nm for panel c and 200 nm for panel d. Numerous pores and tunnels can be observed from Figure c. As shown in Figure d, the diameter of the pores and tunnels are estimated ranging from ~10 to ~100 nm.

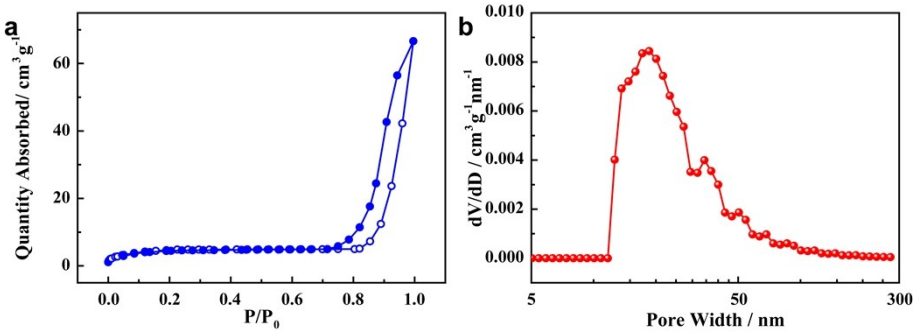

Fig. S5 a) N_2 adsorption/desorption isothermal. b) Pore size distribution analysis of the R-MnNS electrode. To avoid any damage to the $K_{0.3}MnO_2$ porous network, $K_{0.3}MnO_2$ was coated on the SS sheet to form the thin films for the surface area measurements. If only the weight of $K_{0.3}MnO_2$ thin films was calculated, the values of BET surface area and total pore volume are 15.5 $m^2 \cdot g^{-1}$ and 0.1 $cm^3 \cdot g^{-1}$ respectively, which were estimated from Figure a. As shown in Figure b, the $K_{0.3}MnO_2$ thin films show a board peak ranging from ~6.5 to 100 nm corresponding to the mesopores (2 - 50 nm) and macropores (>50 nm).

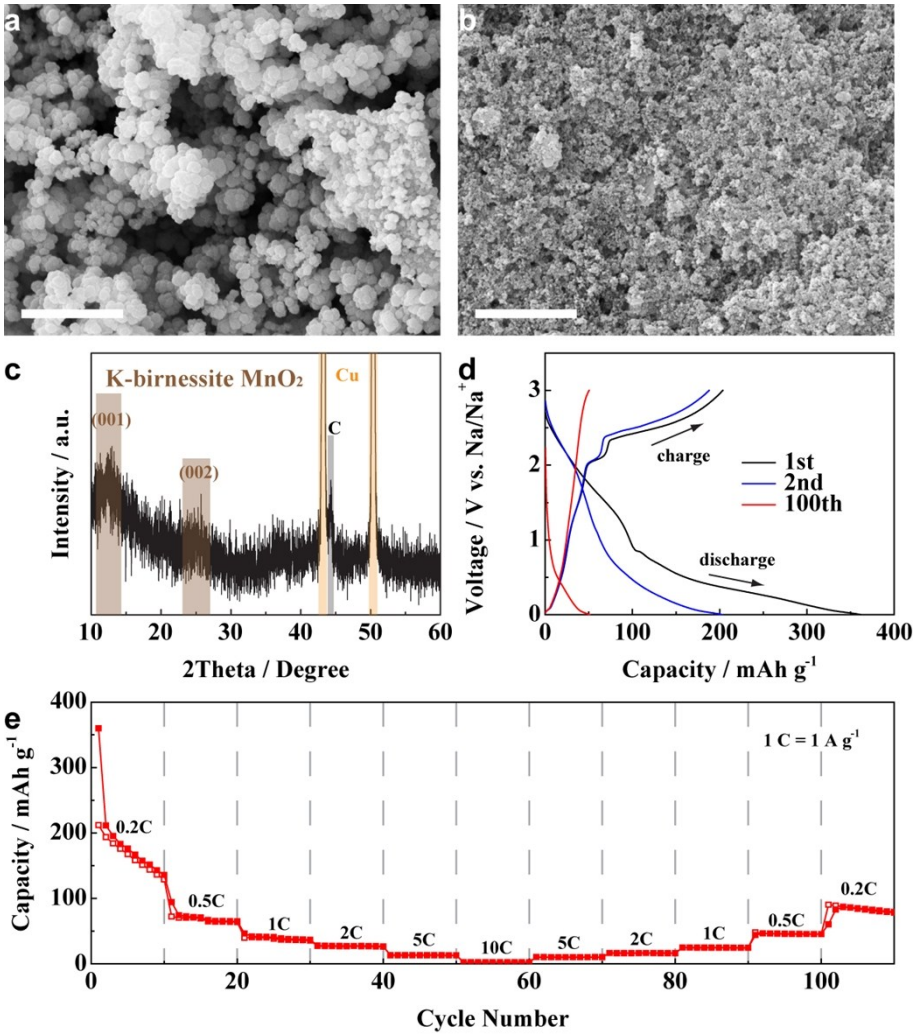

Fig. S6 Na storage mechanism investigation of the K-MnO_2 electrode. a) SEM image of the K-MnO_2 particles. Scale bar is 5 µm. b) SEM images for K-MnO_2 electrode. Scale bar is 5 µm. c) XRD patterns. d) GCD profile for the 1st, 2nd and 100th cycles. e) Rating capability at the current densities of 0.2 - 10 A·g^{-1}.

In Figure S6c, the characteristic peaks at 12.5° and 25° are assigned to the (001) and (002) reflections of the K-birnessite MnO_2 (JCPDS No. 80-1098).

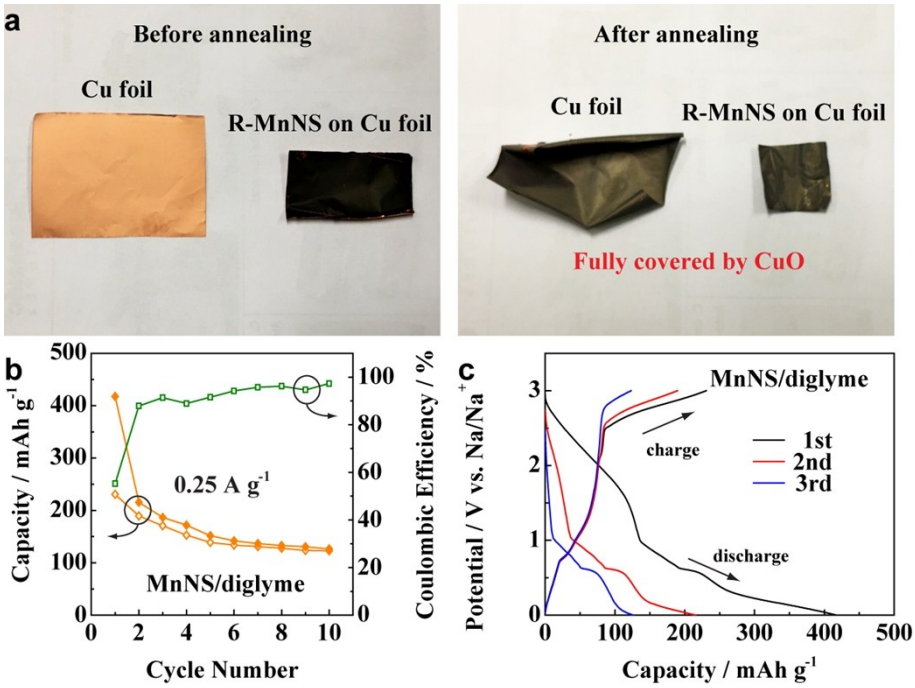

Fig. S7 Substrate influence between Cu foil and SS sheet. a) Optical photos of the Cu foil and R-MnNS on Cu foil before and after annealing at 300 °C in air. b, c) Cyclic performance and corresponding GCD profiles of the MnNS electrode on SS sheet in diglyme-based electrolyte. As shown in Fig. S7c, the GCD profiles of MnNS electrode on SS sheet shows anode-like redox behavior, which could be similar to the GCD profile on Cu foil in Fig. 2e.

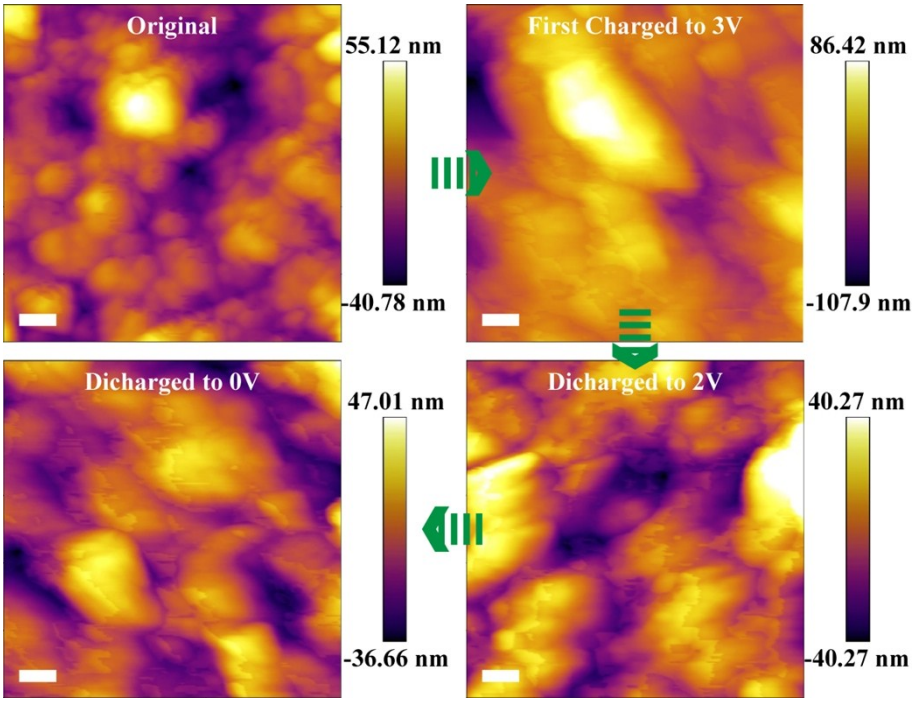

Fig. S8 *In-situ* height profiles at different states measured by AFM. Scale bars are all 100 nm.

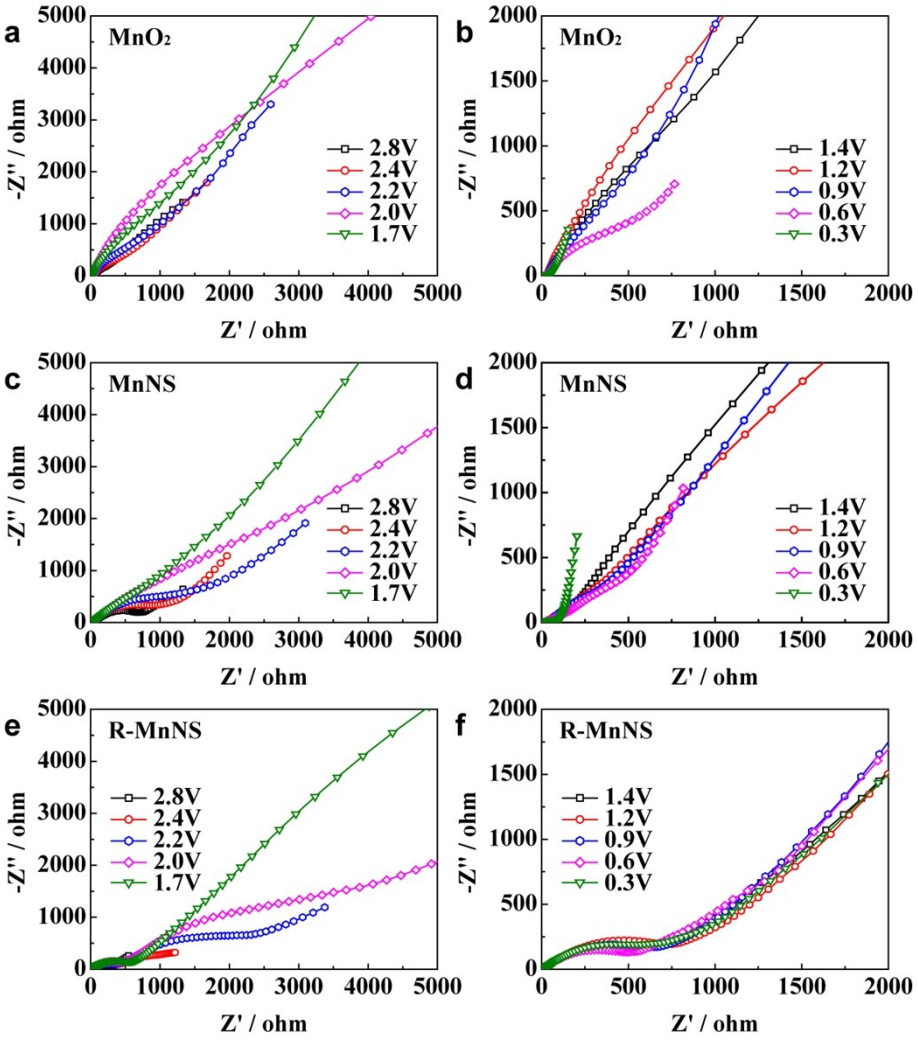

Fig. S9 EIS spectra of the K-MnO_2, R-MnNS and MnNS electrodes at different voltages.

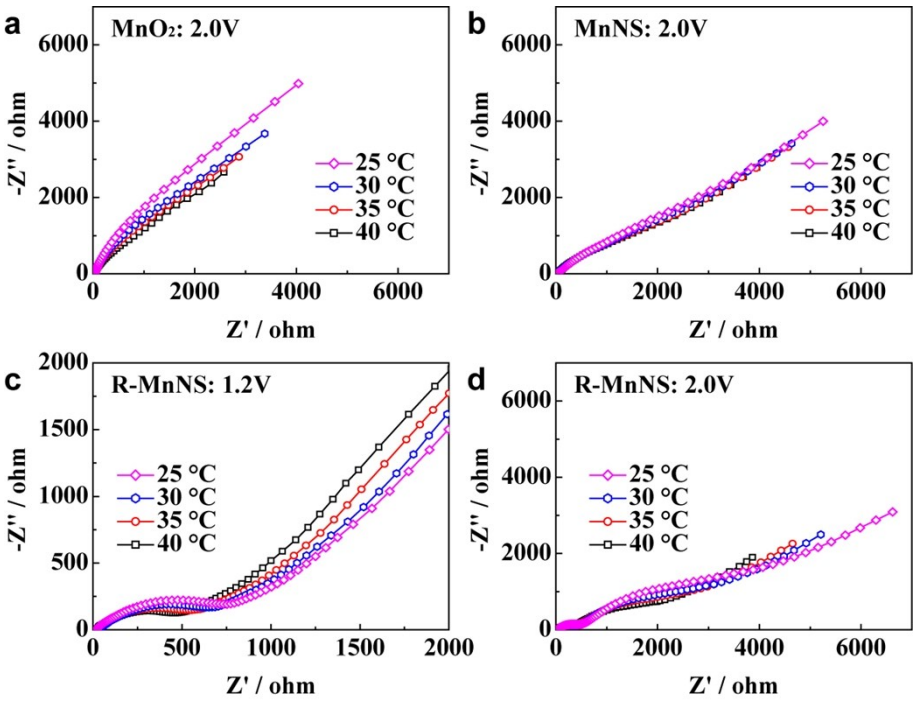

Fig. S10 EIS spectra of the K-MnO_2, R-MnNS and MnNS electrodes at 1.2 and 2 V under different temperatures.

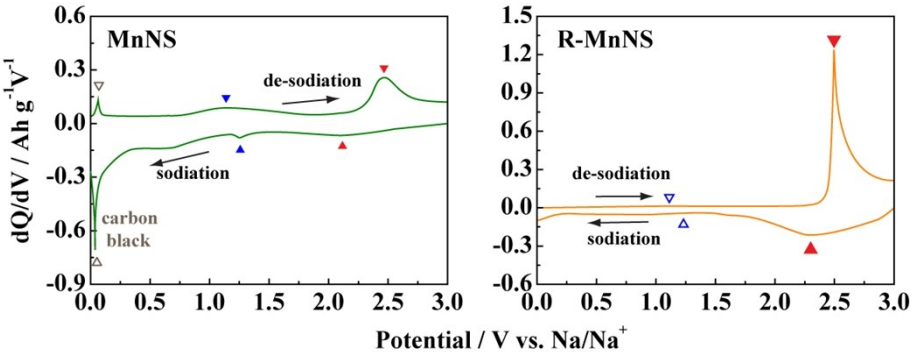

Fig. S11 Differential capacitance plots of the MnNS (left) and R-MnNS (right) electrodes obtained from the second GCD curves.

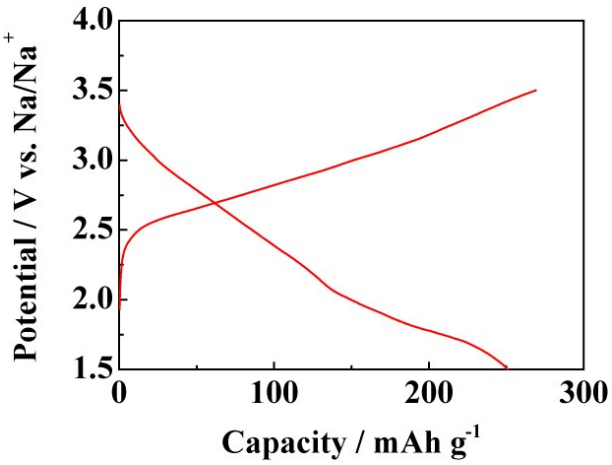

Fig. S12 GCD profile of the R-MnNS electrode in the potential range of 1.5 - 3.5V.

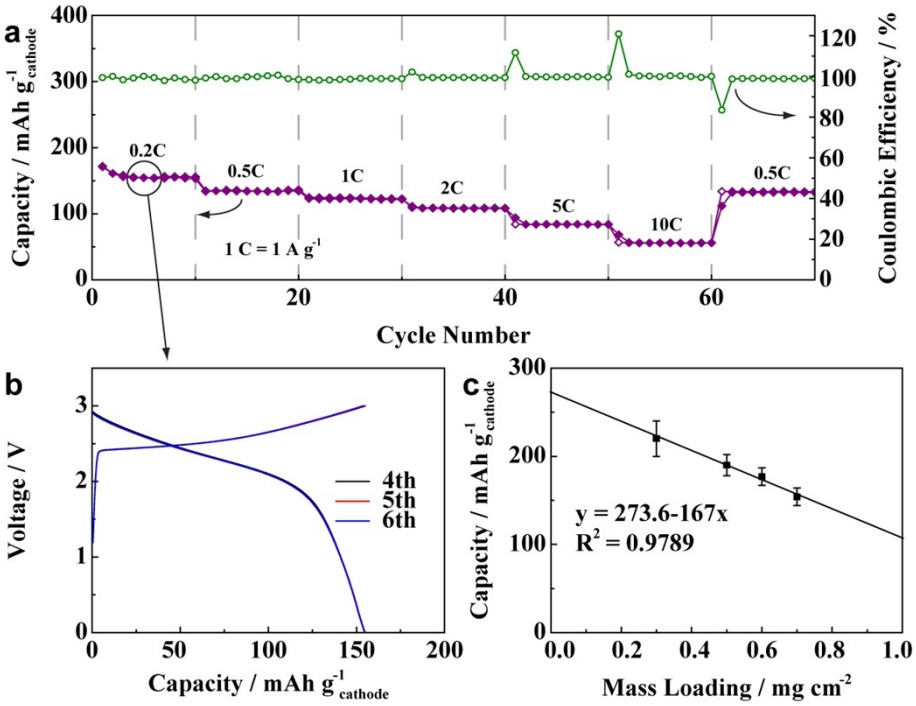

Fig. S13 Electrochemical performance of R-MnNS electrode with high mass loading of 0.7 mg·cm^{-2}. a) Rating performance and coulombic efficiency at 0.2 – 10 A·g^{-1}. b) GCD profiles of the 4th – 6th cycles. c) Capacity versus mass loading of different R-MnNS electrodes at 0.2 A·g^{-1}.

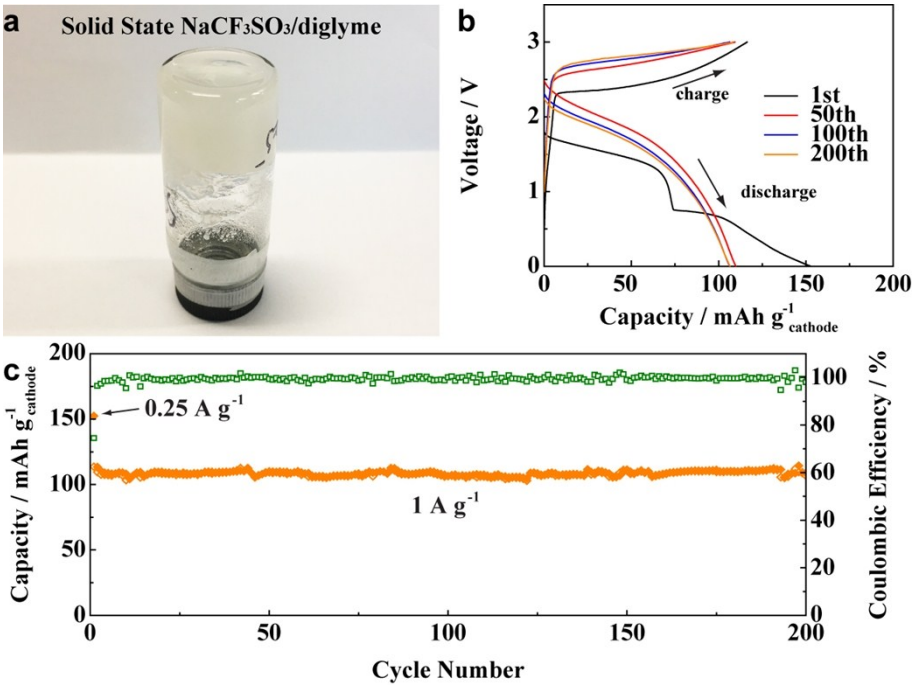

Fig. S14 Cyclic performance of the R-MnNS electrode in gelled diglyme-based electrolyte. a) Optical photograph of the gelled $NaCF_3SO_3$/diglyme electrolyte. b, c) Long term cyclic performance and coulombic efficiency and the corresponding GCD profiles for 200 cycles at 1 $A \cdot g^{-1}$ (0.25 $A \cdot g^{-1}$ for the first cycle).

Recent developments in solid state rechargeable lithium metal batteries inspired us to further explore the solid state sodium metal batteries. As shown in Fig. S14a, to replace the traditional liquid media, the $NaCF_3SO_3$/digylme electrolyte was gelled by using fumed silica nanopowder (mass ratio (liquid electrolyte:silica) = 10:1.5). The R-MnNS cathode and metallic sodium anode were sandwiched with a glass fibers separator and the gelled electrolyte in between. The GCD profiles for the 1st, 50th, 100th and 200th cycles are shown in Fig. S14b. The 1st discharge GCD cycle shows two obvious plateaus at 1.5 and 0.8 V. In the following cycles, the plateau at 0.8 V disappeared and the plateau at 1.5 V moved to ~2.1 V. The charge GCD cycles show one plateau at 2.5 V corresponding to the formation of MnO_2. The cyclic performance and coulombic efficiency were tested at 0.25 $A \cdot g^{-1}$ for the first cycle and at 1 $A \cdot g^{-1}$ for the following cycles, as shown in Fig. S14c. The R-MnNS electrode could achieve a discharge capacity of 152 $mAh \cdot g^{-1}_{cathode}$ for the first cycle (0.25 $A \cdot g^{-1}$) and remain at ca. 110 $mAh \cdot g^{-1}_{cathode}$ when the current density rises to 1 $A \cdot g^{-1}$. The discharge capacity exhibits a slight fluctuation during the cycling but could reach a capacity retention of 96.5% after 200 cycles, indicating a promising potential for practical applications.

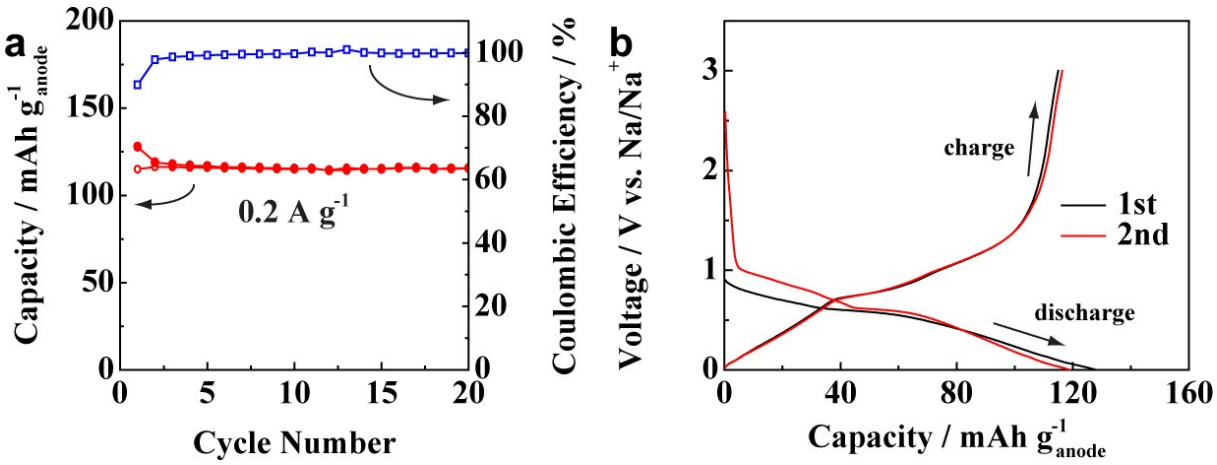

Fig. S15 Cyclic performance of the KS6 carbon electrode. a) Cyclic performance and coulombic efficiency for 20 cycles at 0.2 $A \cdot g^{-1}$. b) GCD profiles for the 1st and 2nd cycles.

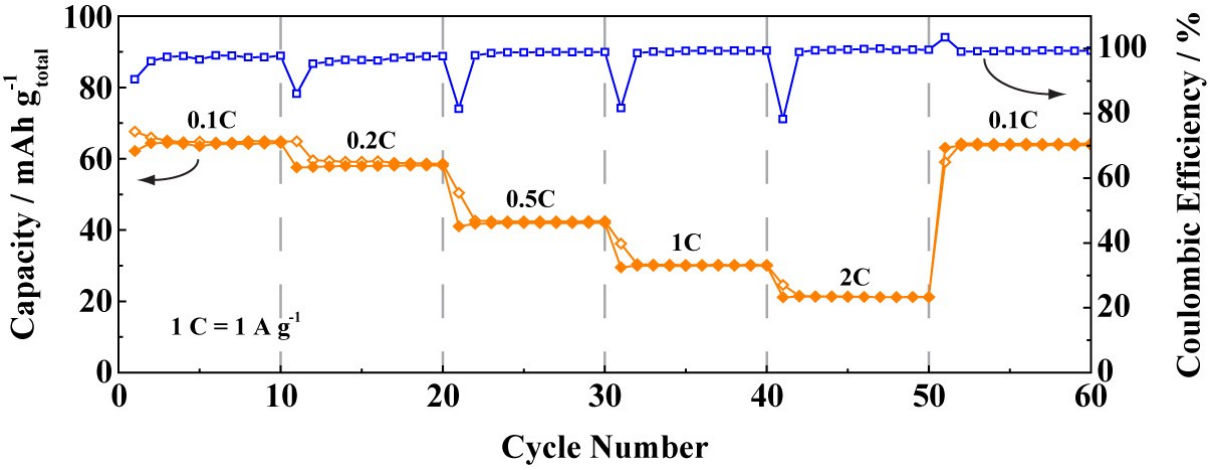

Fig. S16 Rate capability and coulombic efficiency of SR-MnNS//KS6 cell at the current densities of 0.1 - 2 A·g^{-1}.

Table S1. The EIS simulation parameters of the MnNS and R-MnNS electrodes under different conditions.

Electrode	Temperature / °C	Voltage / V	R_s / Ω	R_{SEI} / Ω	R_{ct} / Ω
MnNS	25	2.8	23.14	25.76	601.9
	25	2.4	19.25	32.39	1072
	25	2.2	19.15	30.19	1768
	25	2.0	19.09	28.32	2526
	30	2.0	20.12	24.07	2218
	35	2.0	22.12	18.27	1851
	40	2.0	20.76	13.35	1626
	25	1.7	21.17	21.25	1396
	25	1.4	23.2	14.32	516.6
	25	1.2	18.29	22.39	1641
	25	0.9	20.31	27.57	484.8
	25	0.6	19.94	12.4	576.8
	25	0.3	19.42	10.31	68.19
R-MnNS	25	2.4	18.84	302.6	989.6
	25	2.2	22.21	365.8	2006
	25	2.0	17.53	489.4	3093
	30	2.0	18	400.1	2666
	35	2.0	17.65	351.3	2509
	40	2.0	19.04	291.4	2107

Note: R_s represents the internal resistance of the cell, R_{SEI} and R_{ct} represent the SEI interface and charge transfer resistance.[1, 2] The equivalent circuit that is used to fit the experimental data is shown as follows:

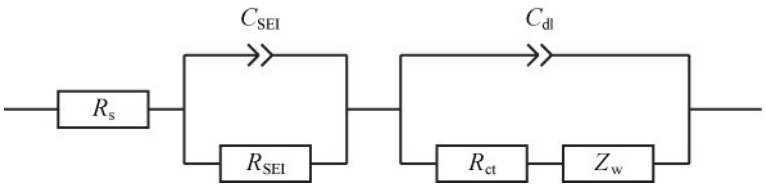

References:

[1] X. Li, J. Rong and B. Wei, *ACS Nano,* 2010, **4**, 6039-6049.

[2] Q. Cheng, J. Tang, J. Ma, H. Zhang, N. Shinya and L. Qin, *Phys. Chem. Chem. Phys.,* 2011, **13**, 17615-17624.